Measurement of neutron capture cross-sections and extraction of neutron resonance parameters at 1—500 eV for ^{109}Ag*

Xie Wen[1], Che Guoliang[1], Jiang Wei[3, 4], Dong Gaoyang[1], Weng Chuxuan[1], Jiang Xin[1], Li Xinxiang[1, 2, *], Feng Song[1, 2, *], Jiang Bing[1, 2], Ren Jie[5], Lin Zi'ang[1], Yin Mingyang[1], Jiang Ting[1], He Rui[1], Wang Hongwei[6, 7], Fan Gongtao[6, 7], Liu Longxiang[6, 7], Zhang Yue[6], Hao Zirui[6], Zhang Suyalatu[8], Wang Dexin[8], Luo Wen[1, 2, *]

1.School of Nuclear Science and Technology, University of South China, Hengyang 421001, China
2.Key Laboratory of Advanced Nuclear Energy Design and Safety, Ministry of Education, Hengyang 421001, China
3.Institute of High Energy Physics, Chinese Academy of Sciences, Beijing 100049, China
4.China Spallation Neutron Source, Dongguan 523803, China
5.China Institute of Atomic Energy, Beijing 102413, China
6.Shanghai Institute of Applied Physics, Chinese Academy of Sciences, Shanghai 201800, China
7.Shanghai Advanced Research Institute, Chinese Academy of Sciences, Shanghai 201210, China
8.Institute of Nuclear Physics, Inner Mongolia Minzu University, Tongliao 028000, China

^{109}Ag is located on the pathway of the slow neutron capture process, and 79% of ^{109}Ag is generated through a rapid neutron capture process. Meanwhile, the mass fraction of ^{109}Ag in Ag-In-Cd control rods is 38.56%. Therefore, the neutron capture cross-section of ^{109}Ag is crucial for both nuclear energy and nuclear astrophysics applications. In this work, a neutron capture cross-section is measured using a ^{109}Ag isotope target at the Back-n white neutron facility of the China Spallation Neutron Source (CSNS). Neutron capture cross-sections in the 1–500 eV energy region are obtained by combining the time-of-flight method and the pulse-height weighting technique. The ^{109}Ag resonance energy, neutron resonance width, and gamma resonance width parameters are extracted using the SAMMY code, which is based on

* The paper is an English translated version of the original Chinese paper published in Acta Physica Sinica. Please cite the paper as: Xie Wen[1], Che Guoliang[1], Jiang Wei[3, 4], Dong Gaoyang[1], Weng Chuxuan[1], Jiang Xin[1], Li Xinxiang[1, 2, *], Feng Song[1, 2, *], Jiang Bing[1, 2], Ren Jie[5], Lin Zi'ang[1], Yin Mingyang[1], Jiang Ting[1], He Rui[1], Wang Hongwei[6, 7], Fan Gongtao[6, 7], Liu Longxiang[6, 7], Zhang Yue[6], Hao Zirui[6], Zhang Suyalatu[8], Wang Dexin[8], Luo Wen[1, 2, *], **Measurement of neutron capture cross-sections and extraction of neutron resonance parameters at 1—500 eV for ^{109}Ag.** *Acta Phys. Sin.*, 2025, 75(2): 020114. DOI: 10.7498/aps.75.20251270

R-matrix theory. The neutron resonance parameters extracted from this study at 139.4 eV are in agreement with the values evaluated in the JENDL-4.0, while the parameters at 169.9 eV and 328.1 eV are in agreement with the values evaluated in the JEFF-4.0. Additionally, the result at 259.3 eV is consistent with the value evaluated in the CENDL-3.2. The datasets presented in this paper are openly available at https://www.doi.org/10.57760/sciencedb.j00213.00197.

^{109}Ag is located on the pathway of the slow neutron capture process, and 79% of ^{109}Ag is generated through a rapid neutron capture process. Meanwhile, the mass fraction of ^{109}Ag in Ag-In-Cd control rods is 38.56%. Therefore, the neutron capture cross-section of ^{109}Ag is crucial for both nuclear energy and nuclear astrophysics applications. In this work, a neutron capture cross-section is measured using a ^{109}Ag isotope target at the Back-n white neutron facility of the China Spallation Neutron Source (CSNS). Neutron capture cross-sections in the 1–500 eV energy region are obtained by combining the time-of-flight method and the pulse-height weighting technique. The ^{109}Ag resonance energy, neutron resonance width, and gamma resonance width parameters are extracted using the SAMMY code, which is based on R-matrix theory. The neutron resonance parameters extracted from this study at 139.4 eV are in agreement with the values evaluated in the JENDL-4.0, while the parameters at 169.9 eV and 328.1 eV are in agreement with the values evaluated in the JEFF-4.0. Additionally, the result at 259.3 eV is consistent with the value evaluated in the CENDL-3.2. The datasets presented in this paper are openly available at https://www.doi.org/10.57760/sciencedb.j00213.00197.

Keywords: neutron capture cross-section, white neutron source, resonance parameter

doi: 10.7498/aps.74.20251270
cstr: 32037.14.aps.74.20251270

1 Introduction

Investigating the origin of elements in the universe has long been a central focus of astrophysics. The cosmological evolution model based on the Big Bang theory successfully explains the formation of light elements, such as hydrogen (H), helium (He), and lithium (Li)[1]. The nucleosynthesis of elements from carbon to iron is well accounted for by nuclear burning processes in stars. However, due to the peak in binding energy per nucleon and the increasing Coulomb barrier, stellar nuclear burning cannot produce elements heavier than iron. Neutron capture reactions serve as the primary mechanism for synthesizing elements beyond iron in the cosmos, as neutrons are electrically neutral and their reaction cross sections generally increase with decreasing system energy. These reactions are categorized into the slow neutron capture process (s-process)[2] and the rapid neutron capture process (r-process)[3]. The s-process predominantly occurs in the helium-burning shells of asymptotic giant branch stars and constitutes the main source of most stable heavy elements beyond iron, such as strontium, barium, molybdenum, and tungsten. In contrast, the r-process requires extreme conditions of very high neutron density, high temperature, and high entropy, typically found in environments with a high neutron-to-seed-nuclei ratio, where neutron capture rates greatly exceed beta-decay rates. Neutron capture cross sections, as a critical parameter in studying neutron capture reactions, play a pivotal role in resolving current discrepancies in research on galactic chemical evolution and elemental abundances[4]. As illustrated in Figure 1, the ^{109}Ag isotope belongs to the lighter heavy elements ($38 < Z < 50$) and lies along the main path of the s-process. Nevertheless, 79% of ^{109}Ag is produced via the r-process[5]. Accurate neutron capture cross section data for ^{109}Ag are essential inputs for calculating astrophysical reaction rates and simulating nucleosynthesis, playing a crucial role in nucleosynthesis network calculations and offering significant reference value for interpreting the observed abundances of cadmium and heavier elements beyond iron.

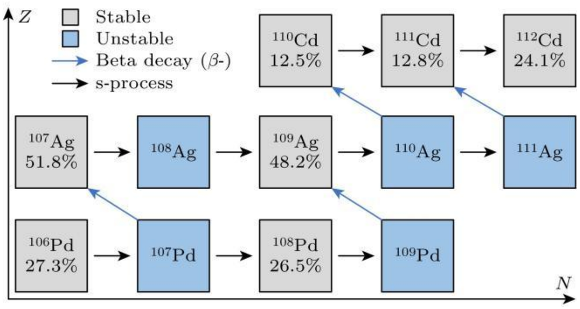

Fig. 1 The s-process reaction path in the region of ^{109}Ag.

Silver-indium-cadmium (Ag-In-Cd) control rods are widely employed in pressurized water reactors. ^{109}Ag constitutes 38.56% by mass and primarily serves to compensate for the excess reactivity of the initial core loading, adjust and maintain reactor operation at a specified power level, and ensure safe shutdown of the core under both normal and emergency conditions[6]. Control rods undergo continuous depletion in high neutron flux environments, causing their inventory to vary as the core fuel is consumed. In early reactor designs, safety margins were relatively large and fuel burnup relatively low, rendering the role of control rods in operational strategies less significant. With growing concerns over energy shortages, reactor designs have increasingly pursued higher fuel burnup to enhance fuel utilization and reduce fuel cycle costs. Consequently, the role of control rods in operational strategies has become increasingly critical[7], necessitating accurate calculation of control rod inventory based on reliable neutron cross-section data for control rod materials.

Currently, five major evaluated nuclear data libraries exist internationally: China's CENDL[8], the United States' ENDF/B[9], Japan's JENDL[10], Europe's JEFF[11], and Russia's BROND[12]. Discrepancies persist among their evaluated neutron capture cross-section data for ^{109}Ag, with deviations approaching two orders of magnitude in the 1-500 eV energy range. According to the International Experimental Nuclear Reaction Data Library (EXFOR)[13], prior experimental measurements of the ^{109}Ag neutron capture cross section have primarily focused on the thermal neutron energy region and the unresolved resonance region, leaving a notable scarcity of precise data in the resolved resonance region. In 2019, Šalamon et al.[14] conducted neutron capture cross-section measurements on natural silver targets at the GELINA facility and extracted neutron resonance parameters for both ^{107}Ag and ^{109}Ag below 1 keV. In 2021, Li et al.[15] extracted resonance parameters for an isotopically enriched ^{107}Ag target in the 1-60 eV range. Compared with Šalamon et al.[14], the radiative resonance widths reported by Li et al.[15] show an average deviation of 1.4% from the ENDF/B-VIII.0 evaluated library, which is smaller than the 4.3% deviation reported by Šalamon et al.[14]. Owing to reduced impurity interference in the target material, experiments employing pure isotopic targets are expected to yield more precise results under identical conditions.

This study presents neutron capture cross-section measurements for ^{109}Ag using a highly enriched isotopic target at the Back-n white neutron experimental facility (Back-n)[17] of the China Spallation Neutron Source (CSNS)[16]. Neutron capture yields for ^{109}Ag were obtained via a C_6D_6 detector system combined with the time-of-flight (TOF) method, from which the neutron capture cross sections were derived. The SAMMY[18] code, based on R-matrix theory, was employed to extract neutron resonance parameters for ^{109}Ag in the 1-500 eV energy range. The experimental workflow for acquiring the relevant data is illustrated in Figure 2.

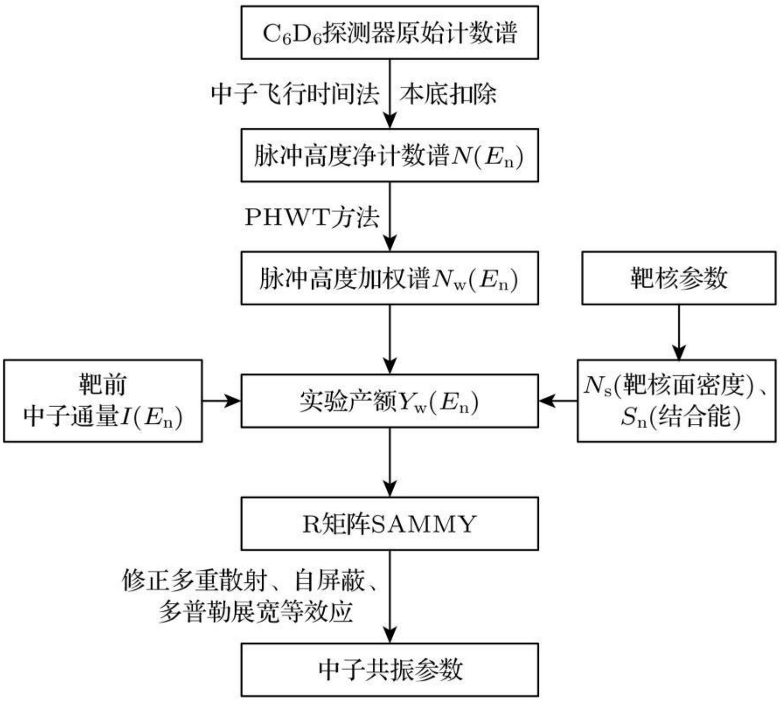

Fig. 2 Procedure for obtaining neutron resonance parameters[16]

2 Experiment and Data Processing

2.1 Experimental Setup

The China Spallation Neutron Source (CSNS) is China's first spallation neutron source facility and serves as a large-scale, multidisciplinary research platform driven by a high-power proton accelerator. Back-n is one of the key experimental stations at CSNS, primarily dedicated to neutron nuclear data measurements and studies of single-event effects induced by high-energy neutrons. Located at the proton beam's back-angle direction (180°) of CSNS, the Back-n beamline extends 80 m in length. Two experimental halls-Experimental Station 1 (ES#1) and Experimental Station 2 (ES#2)-have been constructed along this beamline. ES#2, situated approximately 76 m from the spallation target, achieves a neutron flux of up to 10^7 cm^{-2}/s. The present experiment was conducted at ES#2, with CSNS operating at an average beam power of 100 kW and a repetition frequency of 25 Hz[19]. Four hydrogen-free deuterated benzene (C_6D_6) liquid scintillation detectors (as shown in Figure 3) were employed to detect de-excitation γ-rays produced by neutron capture reactions on a ^{109}Ag isotope target[20]. The pulse height weighting technique (PHWT) was applied to weight the detection efficiency of the γ-rays. Neutron flux upstream of the target was measured using a ^{6}Li-Si detector based on the $^{6}\mathrm{Li}(n,\alpha)^{3}\mathrm{H}$ reaction. In this study, neutron energies were determined using the time-of-flight (TOF) method, as expressed below[21]:

$$E_n = \frac{1}{2} m_n (\frac{L}{t_n})^2, \ (1)$$

Here, m_n denotes the neutron mass, L represents the flight distance, and t_n is the time-of-flight. At the Back-n facility, t_n is calculated using the formula $t_n = (t_{det} - t_\gamma) + L/c$, where t_{det} is the time at which the detector responds to either neutrons or γ-rays, t_γ denotes the arrival time of γ-rays at the detector, and c is the speed of light[22]. In this study, L was set to 76.5 m. The uncertainty in L primarily arises from multiple scattering events occurring within the spallation target[23]. Under the standard operational mode of the China Spallation Neutron Source (CSNS)-the double-bunch pulse mode-each pulse comprises two proton bunches separated by a time interval of 410 ns. Due to the overlapping event distributions associated with the two bunches, direct use of uncorrected data would degrade the time resolution, particularly in the high-energy region, as a consequence of the double-bunch structure[24]. This study employed a pulse-deconvolution method developed by the Back-n collaboration to ultimately obtain data corresponding to a single bunch[25].

The total experimental duration was approximately 70 h. Since the ^{197}Au(n,γ) reaction is internationally recognized as a standard neutron capture cross section[26], a 5 h measurement was performed on a ^{197}Au target to validate the reliability of the experimental setup and data analysis procedures. Measurements of 9.5 h and 6 h were conducted on a natural carbon (^{nat}C) target and an empty target, respectively, to assess the in-beam neutron scattering background and the ambient background[27]. A ^{109}Ag isotopic target was measured for 35.5 h. To calibrate the γ-ray background in the beam, a 4.5 h measurement was carried out using a combination of an aluminum filter and the ^{109}Ag target, followed by a 10 h measurement on a natural lead (^{nat}Pb) target. Detailed information regarding the target parameters is provided in Table 1.

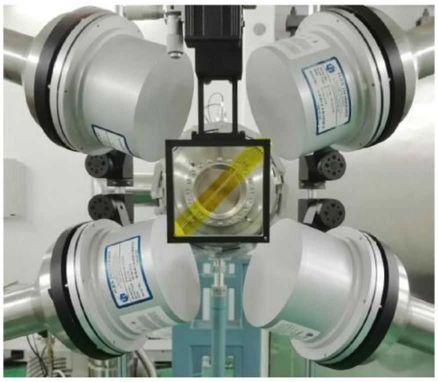

Fig. 3 Photograph of the C_6D_6 detector in the Back-n facility of CSNS.

Table 1. Information of experimental targets.

Experimental target	Purity/%	Diameter/mm	Target thickness/mm	Mass/G
^{109}Ag	>99%	30.00±0.02	0.100±0.005	0.745±0.005
^{197}Au	>99%	30.00±0.02	0.100±0.005	1.423±0.005
^{nat}C	—	30.00±0.02	0.100±0.005	0.160±0.005
^{nat}Pb	—	30.00±0.02	0.100±0.005	0.787±0.005

2.2 Background Subtraction

The background components in neutron capture cross-section measurements using C_6D_6 detectors at Back-n are as follows[28]:

$$B(t) = B_0 + B_{\text{empty}}(t) + B_{\text{sample}}(t), \quad (2)$$

Here, B_0 denotes the background component independent of both the target and time, $B_{\text{empty}}(t)$ represents the time-dependent but target-independent background, and $B_{\text{sample}}(t)$ corresponds to the target-dependent background, which arises from scattering of neutrons and γ-rays by the target. The neutron energy E_{n} is derived from the time-of-flight t:

$$B(E_{\text{n}}) = B_0 + B_{\text{empty}}(E_{\text{n}}) + B_{\text{sn}}(E_{\text{n}}) + B_{\text{s}\gamma}(E_{\text{n}}), \quad (3)$$

Here, $B(E_{\text{n}})$ denotes the total background, while $B_{\text{sn}}(E_{\text{n}})$ and $B_{\text{s}\gamma}(E_{\text{n}})$ represent the backgrounds induced by neutron and γ-ray scattering from the target, respectively.

The background arising from environmental activation and delayed γ rays is independent of both the target and time. This background component, denoted as B_0, was determined by measuring an empty target under beam-off conditions. The background generated by the beam interacting with the environment is independent of the target but varies with time; this component, $B_{\text{empty}}(E_{\text{n}})$, was evaluated by measuring an empty target under beam-on conditions. To measure the background due to scattered neutrons, $B_{\text{sn}}(E_{\text{n}})$, a target with a large scattering cross section over the relevant energy range and a relatively flat neutron capture cross section is required; in this experiment, a carbon target fulfilled these criteria. Lead was selected as the ideal material for assessing the beam-induced γ-ray background, $B_{\text{s}\gamma}(E_{\text{n}})$, because it exhibits a lower neutron capture cross section compared to ^{109}Ag and lacks resonance structures within the relevant energy range[29]. Figure 4 presents the count distributions obtained under the aforementioned measurement conditions, normalized to the neutron fluence.

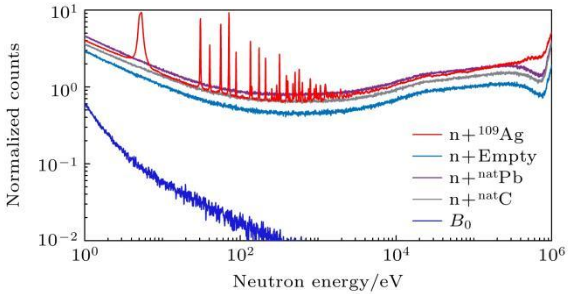

Fig. 4 Normalized experimental energy spectrum.

Since the $B_{s\gamma}(E_n)$ value exhibits no direct correlation with neutron flux, data analysis cannot be performed using counts from the ^{6}Li-Si detector. Therefore, the black resonance method[30] was employed in the experiment to normalize both $B_{sn}(E_n)$ and $B_{s\gamma}(E_n)$. A 40 mm thick ^{27}Al filter was placed at the neutron beam window. The neutron absorption cross section of ^{27}Al displays a double-peak feature at 34.8 keV and 86 keV, effectively attenuating the neutron beam at the corresponding time-of-flight positions. Consequently, the experimental counts at these neutron time-of-flight values arise solely from in-beam gamma rays[31]. Figure 5 presents a comparison of the normalized count spectra for the ^{109}Ag isotope target with and without the filter. Finally, the background for the natural lead target was parameterized as

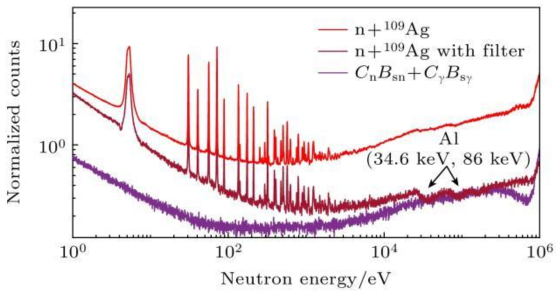

Fig. 5 The ^{109}Ag target with and without filters and background energy spectrum.

$$B_{lead}(E_n) = B_{empty}(E_n) + C_n B_{sn}(E_n) + C_\gamma B_{s\gamma}(E_n). \quad (4)$$

We separately calculated the values of the normalization factor $B_{s\gamma}(E_n)$ for C_γ and the normalization factor $B_{sn}(E_n)$ for C_n.

2.3 Pulse Height Weighting Technique

When the C_6D_6 detector measures prompt γ-rays produced by neutron capture reactions, its detection efficiency is influenced by the complex de-excitation pathways of the compound nucleus[32]. The detector's response function must be processed using the Pulse Height Weighting Technique (PHWT) to render the detection efficiency independent of the energies of cascade γ-rays. In experiments, the detection efficiency of the C_6D_6 detector for capture reactions is approximately equal to the sum of its detection efficiencies for individual cascade γ-rays[21]:

$$\varepsilon_{\mathrm{c}} = 1 - \prod(1 - \varepsilon_{\gamma i}) \approx \sum \varepsilon_{\gamma i}, \quad (5)$$

where ε_{c} denotes the detection efficiency of the C_6D_6 detector for capture reactions, and $\varepsilon_{\gamma i}$ represents the detection efficiency for the i-th cascade γ-ray. Since each $\varepsilon_{\gamma i}$ is sufficiently small, the approximation in Equation (5) holds. Although Equation (5) establishes a relationship between ε_{c} and $\varepsilon_{\gamma i}$, it does not directly manifest in the output pulse height spectrum of the C_6D_6 detector. We aim to establish a direct correlation between ε_{c} and the detector's output spectrum. This would enable direct analysis of ε_{c} from the detector's output signal and subsequent calculation of the neutron capture cross section. Specifically, we require:

$$\varepsilon_{\mathrm{c}} = \alpha \sum E_{\gamma i}, \quad (6)$$

For Equation (6) to hold, the response function of the detection system must be mathematically adjusted to satisfy:

$$\varepsilon_{\gamma i} = \alpha E_{\gamma i}, \quad (7)$$

This approach constitutes the Pulse Height Weighting Technique (PHWT), where α is a proportionality constant and $E_{\gamma i}$ denotes the energy of the cascade γ-ray, which can be directly obtained from the pulse height (PH) spectrum output by the C_6D_6 detector. PHWT was originally proposed by Macklin and Gibbons[33] and applied to C_6F_6 detectors for measuring neutron capture cross sections. After weighting, the total energy of each cascade γ-ray becomes proportional to the weighted detection efficiency, and the normalized detection efficiency is directly reflected in the counts of the pulse height spectrum. Consequently, the detector's efficiency for γ-rays can be characterized through analysis of the pulse height spectrum. This is achieved by introducing a weighting function (WF) that ensures the following equation is satisfied:

$$\int_{\mathrm{EL}}^{\infty} R_{\mathrm{d}}(E_{\mathrm{d}}, E_{\gamma j}) W(E_{\mathrm{d}}) \mathrm{d}E_{\mathrm{d}} = \alpha E_{\gamma j}, \quad (8)$$

where E_L is the threshold of the PH spectrum; E_d is the energy bin of the PH spectrum; $R_d(E_d, E_{\gamma j})$ denotes the counts in the PH spectrum corresponding to the energy response function at E_d; $W(E_d)$ is the weighting factor associated with E_d;

$E_{\gamma j}$ is the energy of the j-th group of γ-rays, and α is set to 1 herein. The weighting function can be expressed as a polynomial function related to the γ-ray energy:

$$\mathrm{WF}(E_{\mathrm{d}}) = \sum_{i=0}^{4} a_i E_{\mathrm{d}}^{i}, \quad (9)$$

where a_i is a parameter of the WF, which can be determined via the least-squares fitting method:

$$\chi^2 = \sum \left(kE_{\gamma j} - \int_{\mathrm{EL}}^{\infty} R_{\mathrm{d}}(E_{\mathrm{d}}, E_{\gamma j})\mathrm{WF}(E_{\mathrm{d}})\mathrm{d}E_{\mathrm{d}}\right)^2. \quad (10)$$

Each event was weighted using an appropriate weighting factor to ensure that the detector's weighted detection efficiency is proportional to the energy of the γ-rays. This study employed the GEANT4 Monte Carlo program[34] to simulate the response of the C_6D_6 detector system to the cascade gamma rays produced by the neutron capture reaction on ^{109}Ag. The raw efficiency curve is shown in Figure 6(a). After applying the weighting function to the raw efficiency, Figure 6(b) clearly demonstrates a linear relationship between the weighted detection efficiency and energy. Furthermore, the ratio of the weighted detection efficiency to energy, displayed in Figure 6(c), approaches unity. Below 1.5 MeV, however, the weighted efficiency no longer remains proportional to energy. Consequently, a threshold must be applied during γ-ray spectrum analysis to eliminate artifacts arising from the breakdown of the weighting function.

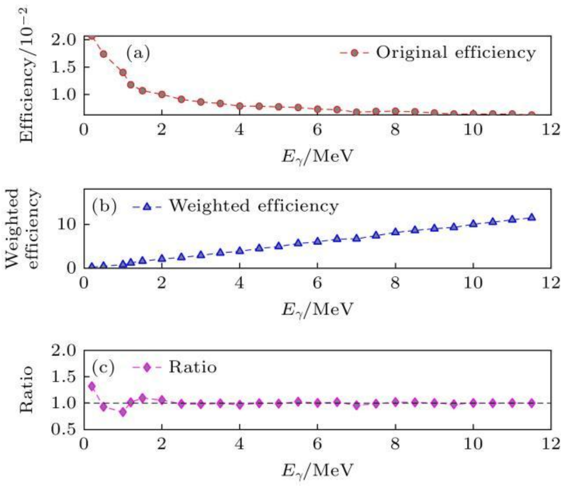

Fig. 6 The C_6D_6 efficiency: (a) Original efficiency; (b) weighted efficiency; (c) the ratio between the weighted efficiency and the γ-ray energy.

2.4 Uncertainty Analysis

Experimental uncertainties arise from experimental conditions, data analysis, and statistical methods. Uncertainties associated with experimental conditions include those from accelerator power, neutron energy spectrum, and target parameters. According to experimental records, the uncertainty contributed by accelerator power in this experiment is less than 1.5%. Based on research by the Back-n collaboration, the energy range covered by the data in this experiment spans 1-500 eV, and the uncertainty introduced by the energy spectrum is less than 8.0%[35]. Uncertainties in target parameters originate from the areal density of the target and the calculation of neutron binding energy, and are influenced by measurements of the target's dimensions, thickness, and mass, as well as the data source for neutron binding energy. This contribution is less than 1.5%. Uncertainties in data analysis include those from normalization, the PHWT method, double-bunch unfolding, and background subtraction. Two primary normalization approaches were employed: The first involves Gaussian fitting of the experimentally measured resonance peak at 30.5-31 eV, followed by comparison of the fitted curve with theoretical data to determine the normalization factor. The second selects the 30.5-31 eV energy interval within the experimental energy range and compares it directly with theoretical data to compute the normalization factor. After calculating the neutron capture cross section using Equation (11), the second resonance peak (30.6 eV) was used to normalize results in the low-energy region. The resulting error in the normalization factor is less than 2.0%. During data analysis, the PHWT method may introduce a systematic error of 2.0%-3.0%[36], while double-bunch unfolding contributes an error of less than 2.0%[25]. The uncertainty from background subtraction stems from the calculation of the normalization factor in the black-resonance method, introducing an uncertainty of less than 2.0%. The statistical uncertainty during the experiment is less than 0.7%. Consequently, the total uncertainty of the experimental results is less than 9.4%, with individual uncertainty contributions listed in Table 2.

Table 2. The sources of uncertainty in experimental measurement.

Sources of uncertainty	Composition	Uncertainty/%
Experimental condition	Accelerator power	<1.5
	Neutron spectrum (< 0.15 MeV)	<8.0
	Target parameter	<1.5
Data analysis	Normalization	<2.0
	PHWT method	<3.0
	Two-bunch deconvolution spectrum	<2.0
	Background Deduction	<2.0
Mathematical statistics	Statistical error	<0.7

3 Results and Discussion

The neutron capture yield is determined by a weighting function. Applying the weighting function (WF) of ^{109}Ag to the net count spectrum-obtained by subtracting the background from the raw data-yields the weighted spectrum $N_{\mathrm{w}}(E_{\mathrm{n}})$. The neutron capture yield $Y_{\mathrm{w}}(E_{\mathrm{n}})$ correlates with $N_{\mathrm{w}}(E_{\mathrm{n}})$, as expressed in reference [37].

$$Y_{\mathrm{w}}(E_{\mathrm{n}}) = \frac{N_{\mathrm{w}}(E_{\mathrm{n}})}{N_{\mathrm{s}} I(E_{\mathrm{n}}) S_{\mathrm{n}}}, \quad (11)$$

Here, N_{s} denotes the areal density of the target, and S_{n} represents the neutron separation energy of the target, with computational data sourced from AME2020[38]. $I(E_{\mathrm{n}})$ is the incident neutron flux at different neutron energies, provided by the Back-n collaboration[35]. The relationship between the neutron capture cross section and the yield is as follows:

$$Y_{\mathrm{w}}(E_{\mathrm{n}}) = (1 - \mathrm{e}^{N\sigma_{\mathrm{t}}(E_{\mathrm{n}})tf_{\mathrm{c}}})\frac{\sigma_{\mathrm{c}}(E_{\mathrm{n}})}{\sigma_{\mathrm{t}}(E_{\mathrm{n}})}, \quad (12)$$

Here, σ_{c} denotes the neutron capture cross section, σ_{c} represents the total neutron cross section, N is the atomic density, and t is the target thickness. Considering that effects such as multiple neutron scattering within the target may cause the actual path length traveled by neutrons to exceed the physical target thickness, a thickness correction factor $f_{\mathrm{c}} = f_{\mathrm{L}}/t$ was introduced, where f_{L} denotes the total path length of neutrons simulated within the target. f_{c} characterizes how the average path length of neutrons varies with neutron energy in a ^{109}Ag target of fixed thickness[36]. This study employed GEANT4 simulations to determine the values of f_{c}, as illustrated in Figure 7.

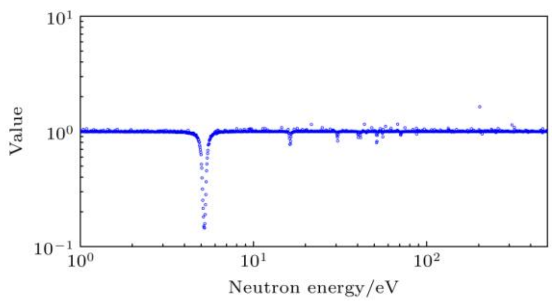

Fig. 7 Variation of the f_{c} with neutron energy.

The neutron capture cross section can be expressed by the following formula:

$$\sigma_c = \frac{N_w}{N_s I S_n} \times \frac{\sigma_t}{(1-e^{N\sigma_t t f_c})}. \quad (13)$$

Figure 8 presents a comparison between the neutron capture cross-section values calculated using Equation (13) and the data compiled in various evaluated libraries. In the energy range of 1-500 eV, the experiment clearly identified 25 neutron resonance peaks, with the lowest cross-section measuring 3.6 b (1 b = 10^{-28} m^2) at 293.2 eV. The experiment did not detect any indication of a neutron resonance for ^{109}Ag at 106.3 eV. According to the evaluated libraries, however, ^{109}Ag exhibits a resonance peak at this energy with a capture cross-section of approximately 7.5 b. Whether a neutron resonance for ^{109}Ag truly exists at this energy requires further experimental verification.

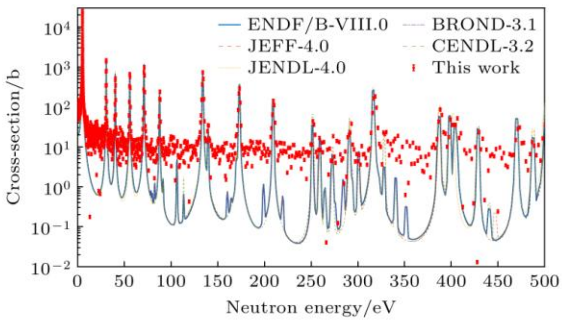

Fig. 8 Calculated cross-section of the experimental data.

For neutron resonances with cross sections exceeding 3.6 b, neutron resonance parameters were extracted using the SAMMY code based on R-matrix theory. The SAMMY code accounts for physical effects including multiple neutron scattering, self-shielding, Doppler broadening, and resonance broadening caused by neutron energy resolution[23]. The capture kernel K is defined as

$$K = g\frac{\Gamma_\gamma \Gamma_n}{\Gamma_\gamma + \Gamma_n}, \quad (14)$$

where Γ_γ denotes the radiation resonance width, Γ_n denotes the neutron resonance width, and the statistical factor g is defined as

$$g = \frac{2J+1}{(2s+1)(2I+1)}, \quad (15)$$

Here, J denotes the total angular momentum, $s = 1/2$ represents the neutron spin, and I is the nuclear spin. This study compares the extracted capture kernel K with those from major evaluated nuclear data libraries.

Figure 9 presents the ratios of the capture kernel K obtained in this study to those calculated using resonance parameters recommended by major evaluated libraries. Since the data from the ENDF/B-VIII.0 and BROND-3.1 libraries are identical, they are represented together by orange hexagons in the figure. Data from the CENDL-3.2, JENDL-4.0, and JEFF-4.0 libraries are denoted by yellow diamonds, purple pentagrams, and green triangles, respectively. The average ratio of our extracted capture kernel K to that computed using ENDF/B-VIII.0 and BROND-3.1 is 1.24, while the corresponding average ratios relative to CENDL-3.2, JENDL-4.0, and JEFF-4.0 are 0.92, 1.23, and 1.02, respectively.

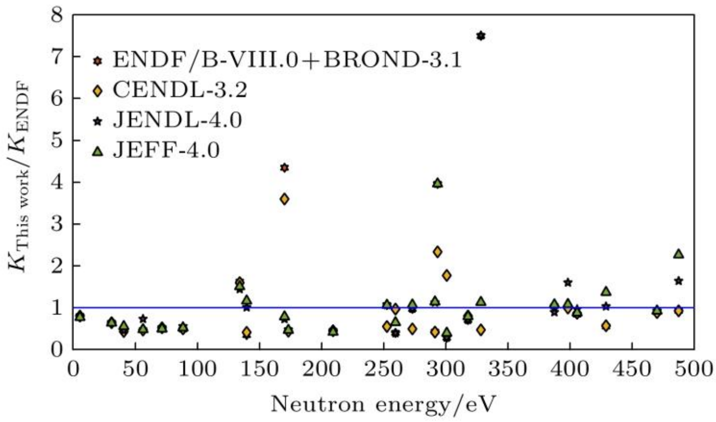

Fig. 9 Comparison between the capture Kernels *K* from the major evaluations and the ones from this work.

The detailed comparison between the experimentally extracted neutron resonance parameters and the data included in major evaluated libraries is presented in Table 3. For convenience in subsequent discussion, the libraries ENDF/B-VIII.0, CENDL-3.2, JENDL-4.0, JEFF-4.0, and BROND-3.1 are denoted as DB#1-5, respectively. Since DB#1 and DB#5 provide identical data at these energy points, they are combined in the table. As shown in Table 3, discrepancies exist among the evaluated libraries regarding the ^{109}Ag neutron resonance parameters at 139.4, 169.9, 259.3, and 328.1 eV. At 139.4 eV, the relative deviations of the experimental Γ_γ values from DB#1-5 are 4%, 4%, 6%, 6%, and 4%, respectively, while those of the experimental Γ_n values are 66%, 60%, 1%, 17%, and 66%, respectively; the experimental results show relatively smaller deviations from the JENDL-4.0 library. At 169.9 eV, the relative deviations of the experimental Γ_γ values from DB#1-5 are 18%, 3%, 3%, 3%, and 18%, respectively, while those of the experimental Γ_n values are 338%, 262%, 27%, 22%, and 338%, respectively; the experimental results show relatively smaller deviations from the JEFF-4.0 library. At 259.3 eV, the relative deviations of the experimental Γ_γ values from DB#1-5 are 19%, 1%, 1%, 1%, and 19%, respectively, while those of the experimental Γ_n values are 63%, 3%, 63%, 36%, and 63%, respectively; the experimental results show relatively smaller deviations from the CENDL-3.2 library. At 328.1 eV, the relative deviations of the experimental Γ_γ values from DB#1-5 are 18%, 3%, 3%, 3%, and 18%, respectively, while those of the experimental Γ_n values are 684%, 56%, 684%, 14%, and 684%, respectively; the experimental results show relatively smaller deviations from the JEFF-4.0 library. Additionally, at 133.8 eV, the relative deviations of the experimentally extracted Γ_γ values from DB#1-5 are 10%, 10%, 17%, 17%, and 10%, respectively, and those of the experimentally extracted Γ_n values are 243%, 234%, 194%, 222%, and 243%, respectively. At 317.7 eV, the relative deviations of the experimentally extracted Γ_γ values from DB#1-5 are 27%, 17%, 21%, 21%, and 27%, respectively, and those of the experimentally extracted Γ_n values are 32%, 23%, 40%, 21%, and 32%, respectively.

Table 3. Comparison of the ^{109}Ag resonance parameters obtained from experiment and the major evaluated libraries.

E_n /eV	Γ_γ /meV					Γ_n /meV				
	This Work	DB#1/#5	DB#2	DB#3	DB#4	This Work	DB#1/#5	DB#2	DB#3	DB#4
5.1	131.11±8.35	130.00	136.00	136.00	135.30	10.02±0.77	12.73	12.70	12.67	13.24
30.6	135.53±3.89	130.00	128.00	130.00	125.50	4.62±0.12	7.33	7.30	7.20	7.38
40.4	151.81±5.30	131.00	131.00	130.00	139.70	2.57±0.07	5.33	6.20	5.87	4.76
55.9	146.22±5.78	139.00	139.00	130.00	130.60	14.94±0.50	37.20	36.80	21.60	36.09
71.2	111.70±5.45	120.00	117.00	130.00	130.00	12.37±0.49	26.67	26.40	25.20	27.49
88.1	149.92±8.18	130.00	131.00	130.00	127.90	2.84±0.11	6.40	6.20	5.47	5.91
133.8	108.54±2.15	120.00	120.00	130.00	130.00	274.05±4.84	80.00	82.00	92.13	85.86
139.4	137.93±12.29	133.00	133.00	130.00	130.00	2.02±0.09	6.00	5.00	2.00	1.73
169.9	133.81±11.21	163.00	130.00	130.00	130.00	1.05±0.04	0.24	0.29	1.44	1.34
173.0	134.96±8.34	140.00	130.00	130.00	130.00	17.42±0.55	44.93	50.00	44.93	46.48
209.0	112.91±9.51	133.00	123.00	130.00	130.00	10.02±1.28	24.00	24.40	24.80	26.36
252.4	123.58±11.90	124.00	130.00	130.00	130.00	6.28±0.54	5.87	11.80	5.87	5.87
259.3	131.94±13.07	111.00	130.00	130.00	130.00	5.03±0.50	13.60	5.20	13.60	7.92
272.9	137.47±13.60	141.00	130.00	130.00	130.00	1.95±0.19	2.00	4.00	2.00	1.82
291.1	132.99±13.10	140.00	140.00	130.00	130.00	12.60±1.11	33.20	34.20	11.07	10.92
293.2	129.80±12.98	163.00	130.00	130.00	130.00	1.67±0.15	0.40	0.68	0.40	0.40
300.6	130.38±12.94	141.00	130.00	130.00	130.00	1.66±0.16	6.00	0.93	6.00	4.27
317.7	102.90±8.91	141.00	124.00	130.00	130.00	121.70±11.33	178.67	158.00	200.00	153.70
328.1	134.04±12.99	163.00	130.00	130.00	130.00	6.82±0.63	0.87	15.40	0.87	6.00
387.3	153.07±13.65	147.00	147.00	130.00	130.00	44.91±4.19	43.33	43.10	55.33	43.02
398.2	140.83±13.94	140.00	140.00	130.00	130.00	22.48±1.96	22.00	22.70	13.33	20.77
405.6	115.84±13.20	146.00	143.00	130.00	130.00	182.11±18.87	200.00	190.00	168.00	210.60
428.9	126.15±12.41	141.00	130.00	130.00	130.00	19.06±1.83	38.00	37.40	18.27	13.32
470.0	120.00±10.92	141.00	134.00	130.00	130.00	129.26±11.96	138.00	148.00	138.00	139.30
487.4	134.34±13.15	141.00	130.00	130.00	130.00	41.76±4.15	45.40	46.80	22.80	15.77

In summary, discrepancies between the experimental results and major evaluated libraries, as well as inconsistencies among different evaluated libraries themselves, are relatively pronounced at the Γ_n values. This indicates substantial differences in the methodologies and standards employed by various evaluated libraries when calculating neutron resonance widths. At 139.4, 169.9, 259.3, and 328.1 eV, the present experimental results align reasonably well with one or several evaluated libraries. However, at 133.8 eV and 317.7 eV, the current data do not sufficiently resolve these discrepancies. Given the current scarcity of experimental data, it is premature to assess the accuracy of either evaluated databases or existing experimental results. We therefore recommend independent experimental verification at 133.8 eV and 317.7 eV.

4 Conclusion

This study measured the neutron capture cross section of ^{109}Ag using the Back-n white neutron source facility at the China Spallation Neutron Source. A pulse-height net count spectrum was obtained via the C_6D_6 detector system and the time-of-flight method, with background contributions subtracted using carbon and lead targets. Applying the Pulse Height Weighting Technique (PHWT), we derived a weighted count spectrum and determined the neutron capture cross section of ^{109}Ag in the energy range of 1-500 eV. The experimentally extracted lower limit for neutron resonance peak cross sections is 3.6 b, observed at 328.1 eV. For resonances exceeding 3.6 b, neutron resonance parameters of ^{109}Ag were extracted using the SAMMY code based on R-matrix theory. At 139.4 eV, the extracted resonance parameters agree with those in the JENDL-4.0 library; at 169.9 eV and 328.1 eV, they align with the JEFF-4.0 library; and at 259.3 eV, they are consistent with the CENDL-3.2 library. Nevertheless, at 133.8 eV and 317.7 eV, the current experimental results do not adequately clarify the observed discrepancies, necessitating further experimental validation.

This work provides experimental neutron capture cross-section data for ^{109}Ag in the resonance energy region and offers experimentally based recommendations at energy points where evaluated libraries diverge. The extracted data can be further applied in fields such as nuclear astrophysics and nuclear reactor design.

Data Availability Statement

The dataset supporting the findings of this study is accessible at the Science Data Bank: https://www.doi.org/10.57760/sciencedb.j00213.00197.

We thank the staff of the China Spallation Neutron Source facility (https://cstr.cn/31113.02.CSNS) and the Back-n white neutron experimental facility (https://cstr.cn/31113.02.CSNS.Back-n) for their technical support and assistance in data collection and analysis.

References

[1] Battino U, Pignatari M, Tattersall A, Denissenkov P, Herwig F 2022 *Universe* **8** 170

[2] Käppeler F, Gallino R, Bisterzo S, Aoki W 2011 *Rev. Mod. Phys.* **83** 157

[3] Thielemann F K, Arcones A, Käppeli R, et al. 2011 *Prog. Part. Nucl. Phys.* **66** 346

[4] Arnould M, Katsuma M 2007 *International Conference on Nuclear Data for Science and*

Technology Nice, France, April 22-27, 2007 p5

[5] Arlandini C, Käppeler F, Wisshak K, Gallino R, Lugaro M, Busso M, Straniero O 1999 *Astron. J.* **525** 886

[6] Lin M, Cheng M S, Dai Z M 2020 *Nucl. Sci. Tech.* **31** 33

[7] Qayyum F, Ali M R, Zahur A, Khan R 2019 *Nucl. Sci. Tech.* **30** 63

[8] Ge Z G, Xu R R, Wu H C, et al. 2020 *EPJ Web Conf.* **239** 09001

[9] Brown D A, Chadwick M B, Capote R, Kahler A C, Trkov A, Herman M W, Sonzogni A A, Danon Y, Carlson A D, Dunn M, et al. 2018 *Nucl. Data Sheets.* **148** 1

[10] Shibata K, Iwamoto O, Nakagawa T, et al. 2011 *Nucl. Sci. Technol.* **48** 1

[11] Hursin M, Xia F, Rochman D 2025 *Nucl. Sci. Eng.* **199** 1987

[12] Blokhin A I, Gai E V, Ignatyuk A V, Koba I I, Manokhin V N, Pronyaev V G 2016 *Yad. Reak. Kon.* **2** 62

[13] Otuka N, Dupont E, Semkova V, et al. 2014 *Nucl. Data Sheets.* **120** 272

[14] Šalamon L, Geslot B, Heyse J, et al. 2019 *Nucl. Instrum. Methods Phys. Res. B* **446** 19

[15] Li X X, Liu L X, Jiang W, et al. 2022 *Chin. Phys. B* **31** 038204

[16] Chen H, Wang X L 2016 *Nat. Mater.* **15** 689

[17] Tang J Y, An Q, Bai J B, Bao J, Bao Y, Cao P, Chen H L, Chen Q P, Chen Y H, Chen Z, et al. 2021 *Nucl. Sci. Tech.* **32** 11

[18] Larson N M 2008 *Oak Ridge National Laboratory Technical Report No*. ORNL/TM-9179/R8

[19] Zhang L Y, Jing H T, Tang J Y, Wang X Q 2016 *Rad. Phys. Chem.* **127** 133

[20] Wang D X, Zhang S Y L T, Jiang W, Ren J, Wang J C, Tang J Y, Ruan X C, Wang H W, Chen Z Q, Huang M R, Tang X, Hu X R, Li X X, Liu L X, Liu B Y, Sun H, Zhang Y, Hao Z R, Song N, Li X, Niu D D, Li G, Meng G F 2022 *Acta Phys. Sin.* **71** 072901

[21] Li X X, Liu L X, Jiang W, et al. 2025 *Nucl. Sci. Tech.* **36** 178

[22] Wang J C, Ren J, Jiang W, et al. 2024 *Nucl. Sci. Tech.* **35** 164

[23] Jiang B, Han J L, Jiang W, Hu J F, Wang X H, Chen J G, Cai X Z 2021 *Nucl. Instrum. Methods Phys. Res. A* **1013** 165677

[24] Liu X Y, Yang Y W, Liu R, et al. 2019 *Nucl. Sci. Tech.* **30** 139

[25] Yi H, Wang T F, Li Y, et al. 2020 *Jour. Instrum.* **15** P03026

[26] Carlson A D, Pronyaev V G, Smith D L, et al. 2009 *Nucl. Data Sheets.* **110** 3215

[27] Li X X, Liu L X, Jiang W, et al. 2021 *Phys. Rev. C* **104** 054302

[28] Ren J, Ruan X, Jiang W, Bao J, Luan G, Zhang Q W, Huang H X, Nie Y B, Ge Z G, An Q, et al. 2021 *Nucl. Instrum. Methods Phys. Res. A* **985** 164703

[29] Ren J, Ruan X C, Chen Y H, Jiang W, Bao J, Luan G Y, Zhang Q S, Huang H X, Wang Z H, An Q, et al. 2020 *Acta Phys. Sin.* **69** 172901

[30] Li X X, Liu L X, Jiang W, et al. 2022 *Phys. Rev. C* **106** 065804

[31] Li X K, An Z D, Jiang W, et al. 2023 *Phys. Rev. C* **108** 035802

[32] Ren J, Ruan X C, Bao J, et al. 2019 *Radiat. Detect. Tech. Meth.* **3** 52

[33] Macklin R L, Gibbons J H 1967 *Phys. Rev.* **159** 1007

[34] Apostolakis J, Arce P, Burkhardt H, et al. 2003 *Nucl. Instrum. Methods Phys. Res. A* **506** 250

[35] Chen Y H, Luan G Y, Bao J, et al. 2019 *Eur. Phys. J. A* **55** 115

[36] Li X X, Liu L X, Jiang W, et al. 2020 *Nucl. Tech.* **43** 080501

[37] Chen Y J, Li X X, Jiang W, et al. 2025 *Phys. Rev. C* **111** 054607

[38] Huang W J, Wang M, Kondev F G, Audi G, Naimi S 2021 *Chin. Phys. C* **45** 030002